Atmos. Chem. Phys. Discuss., 15, 17553–17598, 2015
www.atmos-chem-phys-discuss.net/15/17553/2015/
doi:10.5194/acpd-15-17553-2015

Atmospheric Chemistry and Physics Discussions
Open Access

Modelling marine emissions and atmospheric distributions of halocarbons and DMS: the influence of prescribed water concentration vs. prescribed emissions

S. T. Lennartz[1], G. Krysztofiak-Tong[2,a], C. A. Marandino[1], B.-M. Sinnhuber[2], S. Tegtmeier[1], F. Ziska[1], R. Hossaini[3], K. Krüger[4], S. A. Montzka[5], E. Atlas[6], D. Oram[7], T. Keber[8], H. Bönisch[8], and B. Quack[1]

[1]GEOMAR Helmholtz-Centre for Ocean Research Kiel, Kiel, Germany
[2]Karlsruhe Institute of Technology, Institute for Meteorology and Climate Research, Karlsruhe, Germany
[3]School of Earth and Environment, University of Leeds, Leeds, UK
[4]University of Oslo, Department of Geosciences, Oslo, Norway
[5]NOAA/CMDL, Boulder, CO, USA
[6]RSMAS/MAC, University of Miami, Florida, USA
[7]University of East Anglia, School of Environmental Sciences, Norwich, Norfolk, UK

[8]Goethe University Frankfurt a.M., Institute for Atmospheric and Environmental Sciences, Frankfurt, Germany
[a]now at: LPC2E, UMR 7328, CNRS-Université d'Orléans, 45071 Orléans CEDEX 2, France

Received: 24 April 2015 – Accepted: 02 June 2015 – Published: 30 June 2015

Correspondence to: S. T. Lennartz (slennartz@geomar.de)

Published by Copernicus Publications on behalf of the European Geosciences Union.

Abstract

Marine produced short-lived trace gases such as dibromomethane (CH_2Br_2), bromoform ($CHBr_3$), methyliodide (CH_3I) and dimethylsulfide (DMS) significantly impact tropospheric and stratospheric chemistry. Describing their marine emissions in atmospheric chemistry models as accurately as possible is necessary to quantify their impact on ozone depletion and the Earth's radiative budget. So far, marine emissions of trace gases have mainly been prescribed from emission climatologies, thus lacking the interaction between the actual state of the atmosphere and the ocean. Here we present simulations with the chemistry climate model EMAC with online calculation of emissions based on surface water concentrations, in contrast to directly prescribed emissions. Considering the actual state of the model atmosphere results in a concentration gradient consistent with model real-time conditions at ocean surface and atmosphere, which determine the direction and magnitude of the computed flux. This method has a number of conceptual and practical benefits, as the modelled emission can respond consistently to changes in sea surface temperature, surface wind speed, sea ice cover and especially atmospheric mixing ratio. This online calculation could enhance, dampen or even invert the fluxes (i.e. deposition instead of emissions) of VSLS. We show that differences between prescribing emissions and prescribing concentrations (−28 % for CH_2Br_2 to +11 % for $CHBr_3$) result mainly from consideration of the actual, time-varying state of the atmosphere. The absolute magnitude of the differences depends mainly on the surface ocean saturation of each particular gas. Comparison to observations from aircraft, ships and ground stations reveals that computing the air–sea flux interactively leads in most of the cases to more accurate atmospheric mixing ratios in the model compared to the computation from prescribed emissions. Calculating emissions online also enables effective testing of different air–sea transfer velocity parameterizations k, which was performed here for eight different parameterizations. The testing of these different k values is of special interest for DMS, as recently published parameterizations derived by direct flux measurements using eddy covariance

ACPD
15, 17553–17598, 2015

measurements suggest decreasing k values at high wind speeds or a linear relationship with wind speed. Implementing these parameterizations reduces discrepancies in modelled DMS atmospheric mixing ratios and observations by a factor of 1.5 compared to parameterizations with a quadratic or cubic relationship to wind speed.

1 Introduction

The oceans emit large amounts of halogen (Penkett et al., 1985; Quack and Wallace, 2003) and sulfur containing substances (Bates et al., 1992; Watts, 2000) that influence atmospheric chemistry. Organic bromine and iodine in the atmosphere is largely supplied by oceanic emissions of Very Short Lived Substances (VSLS) such as dibromomethane (CH_2Br_2), bromoform ($CHBr_3$) and methyliodide (CH_3I) (Lovelock and Maggs, 1973; Hossaini et al., 2013). Also, a large fraction of the atmospheric sulfur loading is due to oceanic emissions of OCS, CS_2, H_2S and dimethyl sulphide (DMS, CH_3SCH_3), the latter being the major compound transporting sulfur from the ocean to the atmosphere (Watts, 2000; Sheng et al., 2015).

Assessing marine emissions of VSLS is crucial, as they significantly influence the Earth's atmosphere in both the troposphere and the stratosphere. In the troposphere, bromine containing VSLS such as $CHBr_3$ and CH_2Br_2 contribute effectively to ozone destruction and alter the oxidative capacity (von Glasow et al., 2004; Salawitch, 2006). Oceanic CH_3I is the main organic iodine compound in the atmosphere (Lovelock and Maggs, 1973), and impacts tropospheric oxidative capacity and ozone destruction (Chameides and Davis, 1980; Saiz-Lopez et al., 2012). DMS emitted to the troposphere is a precursor of secondary organic aerosol and potentially cloud condensation nuclei and thus influences the radiative budget (Charlson et al., 1987). Halogenated VSLS also enhance stratospheric ozone depletion and thus contribute to the ozone-driven radiative forcing of climate (Hossaini et al., 2015). Despite the short lifetime of CH_3I (4–7 days) compared to the bromocarbons (6–120 days), there is potential for a small fraction of marine produced CH_3I to be transported to the stratosphere where it also

ACPD
15, 17553–17598, 2015

contributes to ozone depletion (Tegtmeier et al., 2013; Solomon et al., 1994). DMS has a shorter lifetime (~ 1 day) compared to CH_3I, but there is potential even for the very short lived DMS to be transported to the tropical tropopause layer (TTL) in convective hot spot regions (Marandino et al., 2013a, b).

The impact of marine VSLS emissions on atmospheric chemistry has been studied in chemistry-climate and transport models (e.g. Salawitch et al., 2005; Kerkweg et al., 2006b; Sinnhuber et al., 2009; Liang et al., 2010; Ordóñez et al., 2012). Therein, marine emissions of the VSLS have mainly been based on prescribed boundary layer mixing ratios (Aschmann et al., 2009) or emission scenarios (Warwick et al., 2006; Liang et al., 2010; Ordóñez et al., 2012; Hossaini et al., 2013). However, prescribing emissions in atmospheric models lacks the impact of the atmospheric boundary layer mixing ratio on the concentration gradient. This concentration gradient at the interface between ocean and atmosphere directly influences the emissions, as it determines the direction and magnitude of the flux. The lack of potential feedbacks can result in a modelled atmospheric concentration inconsistent with the oceanic surface concentration.

Here, we evaluate a conceptually different way of considering marine emissions in chemical climate models that is based on a consistent concentration gradient between ocean and atmosphere. Compared to the previous approaches of either specifying atmospheric surface mixing ratios or specifying sea-to-air fluxes, water concentrations are prescribed and emissions are calculated online. Thus, the concentration gradient at the interface and the emissions are consistent with the atmospheric boundary layer and the ocean surface, and the emissions can respond to the actual state of the atmosphere. The approach is applied to established concentration climatologies of short lived halocarbons (CH_2Br_2, $CHBr_3$, CH_3I) and sulfur compounds (DMS) that share common characteristics such as supersaturation in the surface ocean and marine production. For the halocarbons, this set-up is applied for the first time and uses surface ocean concentration climatologies derived from observations by Ziska et al. (2013). DMS emissions have been modelled online previously during a test for the implementation of different submodels (Kerkweg et al., 2006b), but not with the most updated

ACPD
15, 17553–17598, 2015

concentrations prescribed from Lana et al. (2011) and without comparison to observations from aircraft and ship campaigns as in this study.

Prescribing water concentrations and calculating emissions online enables convenient testing of different air–sea gas exchange parameterizations. Air-sea gas exchange is calculated as the product of the concentration gradient between air and water at the surface and the transfer velocity. The latter needs to be parameterized, and many different parameterizations have been published (see e.g. Wanninkhof et al., 2009 for a summary). Most parameterizations relate the transfer velocity to wind speed (e.g. Liss and Merlivat, 1986; Wanninkhof and McGillis, 1999; Nightingale et al., 2000; Ho et al., 2006), but others take the effect of bubble mediated transfer (Asher and Wanninkhof, 1998) or enhancement by rain (Ho et al., 1997, 2004) into account. Testing a variety of different parameterizations on prescribed water concentrations to calculate atmospheric abundances provides information on the uncertainties of global emission estimates.

The experimental set-up consists of two steps: first, we prescribed surface water concentrations in the chemistry climate model EMAC (ECHAM5/MESSy for Atmospheric Chemistry) (Jöckel et al., 2006, 2010) and air–sea exchange of VSLS was then calculated online by the submodel AIRSEA (Pozzer et al., 2006). The model results are then evaluated and compared to a simulation where the difference results from prescribed VSLS emissions (PE). To obtain a comparable set-up, we use water concentration climatologies and corresponding emissions climatologies by Ziska et al. (2013) for halocarbons and Lana et al. (2011) for DMS. The modelled atmospheric mixing ratios of the gases are compared to measurements from time series of ground based stations, ship and aircraft campaigns in order to identify whether the online calculation is simulating the atmospheric mixing ratios more accurately. In a second step, we use the coupled module to test the sensitivity of the global emissions towards eight different, frequently used or recently published, transfer velocity parameterizations.

ACPD
15, 17553–17598, 2015

2 Model set-up and data description

2.1 The atmosphere-chemistry model EMAC

The ECHAM5/MESSy Atmospheric Chemistry (EMAC) model is a global atmospheric chemistry climate model described in Jöckel et al. (2006, 2010). EMAC/MESSy includes submodels describing processes of the troposphere and middle atmosphere as well as interaction with land and human influences. Air-sea gas exchange is calculated in EMAC with the submodul AIRSEA, as described by Pozzer et al. (2006).

The numerical simulations were nudged towards the European Centre for Medium-Range Weather Forecasts (ECMWF), ERA-Interim reanalysis (Dee et al., 2011) every 6 h (temperature, divergence, vorticity, surface pressure). The resolution of the EMAC atmosphere was $\sim 2.8^{\circ} \times 2.8^{\circ}$ (T42) and 39 vertical hybrid pressure levels up to 0.01 hPa (L39). The atmospheric model as well as the submodel AIRSEA uses a time step of 600 s. The convective transport follows the scheme of Tiedtke (1989) and the tracer advection is described in Lin and Rood (1996). An overview on these nudged simulation set-ups can be found in Sect. 2.3.

The simulations include the four very short lived species CH_2Br_2, $CHBr_3$, CH_3I and DMS and simplified atmospheric loss reactions for them. The loss reactions include:

- oxidation with OH, $O(^1D)$, Cl and photolysis for $CHBr_3$ and CH_2Br_2 following the reactions rates by Sander et al. (2011),
- oxidation with OH, Cl and photolysis for CH_3I (Sander et al., 2011),
- and oxidation with OH and $O(^3P)$ for DMS (Sander et al., 2011).

EMAC uses monthly mean concentrations of OH, developed and evaluated for the TRANSCOM-CH4 model intercomparison project, and discussed in detail by Patra et al. (2014). Photolysis rates for VSLS were calculated by the TOMCAT CTM which has been used extensively to examine the tropospheric chemistry of VSLS (e.g. Hossaini et al., 2013). These fields have recently been used and evaluated as part of the

ACPD
15, 17553–17598, 2015

ongoing TRANSCOM-VSLS model intercomparison project (http://www.transcom-vsls.com). The simulated atmospheric lifetimes in our set-up generally agree well with published estimates for these gases, indicating that the basic assumption of the simplified chemistry applied here is valid. The local mean tropical (20° N–20° S) lifetime of CH_2Br_2 in the troposphere in our model study is 143 days and thus lies below 167 days as in Hossaini et al. (2010). The mean tropospheric tropical lifetime of $CHBr_3$ is 20 days in our study, which is consistent within 10 % with a recent reevaluation of $CHBr_3$ lifetime by Papanastasiou et al. (2014), together with a recent reevaluation of the reaction of OH with $CHBr_3$ by Orkin et al. (2013). The local lifetime of CH_3I in our study is 3 days which is in accordance with the study of Tegtmeier et al. (2013). The DMS lifetime in the boundary layer of about 3 days is consistent with the values reported by Notholt and Bingemer (2006).

2.2 Parameterizations of air–sea gas exchange

In this study, the AIRSEA submodel (Pozzer et al., 2006) and its approach for air–sea gas exchange was adopted, using the two layer model (Liss and Slater, 1974). Marine emissions F of gases are calculated as the product of the concentration gradient between air and water concentration of the gas (Δc) and the transfer velocity k (Eq. 1), which needs to be parameterized.

$$F = k \cdot \Delta c = k \cdot (c_{\mathrm{w}} - H \cdot c_{\mathrm{air}}) \tag{1}$$

with c_{w} being the water concentration, H the Henry-constant (dimensionless, water over air) and c_{air} the concentration of the gas in air which was taken from the modelled atmosphere in the respective time step. Henry constants and their temperature dependencies are taken from Moore et al. (1995) for the halocarbons and De Bruyn et al. (1995) for DMS.

The transfer velocity k comprises air- (k_{air}) and water-side (k_{w}) transfer velocities (Eq. 2) in all parameterizations with the Henry constant H, temperature T and the ideal

ACPD
15, 17553–17598, 2015

gas constant R:

$$k = \left(\frac{1}{k_w} + \frac{R \cdot H \cdot T}{k_{air}} \right)^{-1} \quad (2)$$

The water-side transfer velocitiy k_w is often parametrized in relation to wind speed with linear (e.g. Liss and Merlivat, 1986), quadratic (e.g. Ho et al., 2006) or cubic (e.g. Wanninkhof and McGillis, 1999) dependencies. Differences between these parameterizations arise from different techniques to determine k_w, for instance dual tracer techniques (e.g. Nightingale et al., 2000; Ho et al., 2006) or direct flux measurements with eddy covariance (Marandino et al., 2009; Bell et al., 2013). Additional drivers of gas exchange, e.g. bubble mediated transfer (e.g. Asher and Wanninkhof, 1998) and enhancement in the presence of rain (e.g. Ho et al., 2004) are discussed. Bubble mediated transfer has been suggested to be influential for gases with low solubilities, since they more quickly escape from the liquid phase into the bubbles. Bubbles are more easily transported to the surface and released to the atmosphere, thereby adding to the total flux. Rain is believed to add to the flux under calm wind conditions due to an alteration of the sea surface (Ho et al., 2004).

For sparingly soluble gases, k_w dominates the transfer velocity, and k_{air} is often neglected as a simplification. For more soluble gases, McGillis et al. (2000) found that considering k_{air} alters the flux to the atmosphere significantly when low temperatures or moderate wind speeds prevail. Parameterizations of k_{air} assume e.g. a dependency on the friction velocity and surface wind speed (Kerkweg et al., 2006a). k_{air} consistent with Kerkweg et al. (2006a; Eqs. 3 and 4 therein) is considered in the AIRSEA submodel.

The transfer velocity needs to be adapted to each gas by scaling it with the dimensionless Schmidt number in water for k_w and the Schmidt number in air for k_{air} divided by the Schmidt number that the specific parameterization was normalized to, which is in most cases either 600 or 660. The Schmidt number is the ratio of the diffusion coefficient of the compound to the kinematic viscosity of the surrounding medium. Following

ACPD
15, 17553–17598, 2015

the approach of the AIRSEA submodel, the Schmidt number in water is estimated by scaling the CO_2 Schmidt number in water (Wanninkhof et al., 1992; Wilke et al., 1955), while the Schmidt number in air is calculated from air viscosity and diffusivity of the gas in air (Lymann et al., 1990).

2.3 Experimental Set-up

2.3.1 Prescribed concentrations and prescribed emissions

The experimental set-up consists of two steps: first, we compare emissions and atmospheric mixing ratios from prescribed water concentrations (PWC) with those derived from prescribed emissions (PE) (Fig. 1). For the PWC and PE set-up, two different submodels are used to calculate the emissions in EMAC: in the PE approach, emission climatologies are prescribed offline using the submodel OFFLEM (Kerkweg et al., 2006b). For the PWC set-up, emissions (or depositions) are calculated online using the submodel AIRSEA (Pozzer et al., 2006). Details of the simulation set-ups for the simulation 1 (PWC) and 2 (PE) can be found in Table 1. Both simulations cover a period of 24 years (1990–2013) to average out interannual variabilities in emissions and to ensure that the model output can be subsampled specifically at the times of atmospheric observations specified in Sect. 2.4.

In simulation 1 (PWC), we prescribe water concentration climatologies for the halocarbons from Ziska et al. (2013; Z13), and for DMS from Lana et al. (2011, L11). The assumption of constant water concentrations despite loss by emissions is justified by the relatively small emissions compared to the absolute amount of gas in the oceanic mixed layer and the fast production of the compounds in water (e.g. Hopkins and Archer, 2014; Hepach et al., 2015). The modelled emissions from the PWC set-up are compared to the original Z13/L11 emission climatologies. In the same manner, resulting atmospheric mixing ratios in the PWC simulation are compared to atmospheric concentrations from the PE set-up with prescribed emissions from Z13/L11. The emission climatology from Z13 is based on constant water and atmospheric concentra-

ACPD
15, 17553–17598, 2015

tions extrapolated from ~ 5000 measurements, using ERA-Interim wind fields and the Nightingale et al. (2000) parameterization for water-side transfer velocity. The L11 concentration climatology is based on ~ 40 000 measurements and surface wind data for the emission climatologies from the NCEP/NCAR reanalysis project with a water-side transfer velocity parametrized according to Nightingale et al. (2000, N00) and an air-side transfer velocity according to Kondo (1975). The climatologies, prescribing emissions and concentrations of the gases of interest (CH_2Br_2, $CHBr_3$, CH_3I and DMS) were regridded to the T42 grid of EMAC with ncregrid (Jöckel, 2006), which is in all four cases coarser than the original grid described in Z13/L11. It has to be noted that this leads to a smoothing of small, local hotspots, but we assume this to be negligible since we compare emissions on a global scale.

Besides the concentrations taken from the climatologies Z13/L11, the air–sea calculation requires information on sea surface temperature, salinity and wind. The mean sea surface temperature in the model for simulation 1 (1990–2013) was 15.95 °C, 15.82 °C in Z13 and 16.22 °C in L11. The mean wind speed in the model was 7.51 $m\,s^{-1}$, 4.7 % larger than in Z13 and 2.7 % larger than in L11. Sea surface salinity is prescribed with a constant value of 0.4 $mol\,L^{-1}$ in our model simulations opposite to spatially varying salinity in Z13/L11. A two-year simulation comparing the effects of a constant salinity vs. the Z13 climatology revealed a low effect on global emissions (< 3 %), which is in accordance with findings of Ziska et al. (2013). Compared to the calculation of the Schmidt number in the publications by Z13/L11, the submodel AIRSEA uses a different empirical, temperature dependent equation to calculate the Schmidt number. In AIRSEA, the Schmidt number of CO_2 at the respective temperature is calculated and then adapted with the molar volume to the Schmidt number of the gas of interest (Wilke, 1955; Hayduk and Laudie, 1974). In Z13, the Schmidt number is calculated by averaging the diffusion coefficient according to Hayduk and Laudie (1974) and Wilke and Chang (1955) and then dividing by the dynamic viscosity of seawater at varying temperatures and a constant salinity of 35. In L11, the Schmidt number is calculated according to Saltzman et al. (1993). The resulting differences

ACPD
15, 17553–17598, 2015

are negligible at sea surface temperatures higher than 10 °C and grow largest at 0 °C, where they are still less than 15 %. Since the Schmidt number is then normalised to the Schmidt-number of CO_2, the resulting difference becomes small and does not lead to significant differences in the global emission estimates of all four compounds. Differences in other influential input parameters for emission calculation between our PWC set-up and Z13/L11 are thus small, ensuring that differences in emissions between PWC and Z13/L11 can be attributed to the consideration of the actual state of the atmosphere in the PWC set-up.

2.3.2 Transfer velocity parameterizations

In the second part of the study, we test the sensitivity of the global emissions towards eight different transfer velocity parameterizations. These tests cover a two year time span (2010–2011) with one year (2009) as spin-up. The simulations 3–6 (Table 1) test the impact of different water-side transfer velocity parameterization related to wind speed. The parameterizations tested in this study are illustrated in Fig. 2. With increasing wind speed, the differences between the transfer velocity parameterizations grow larger; hence testing these parameterizations yields a range of global emission estimates that reflects this uncertainty. Parameterizations and the general description of air–sea gas exchange calculation are described in Sect. 2.2.

Table 1 provides an overview on all performed simulations. Simulation 3 uses the 3-step linear parameterization of Liss and Merlivat (1986, LM86), simulation 4 the cubic relationship by Wanninkhof and McGillis (1999, W99), simulation 5 the quadratic parameterization by Nightingale et al. (2000, N00), and simulation 6 the quadratic transfer velocity parameterization by Ho et al. (2006, H06). The effect of rain (simulation 7 in Table 1) was tested adding the Ho et al. (1997) rain effect parameterization to the H06 transfer velocity parameterization (see Pozzer et al., 2006, Eqs. 10 and 11). White cap coverage according to Asher and Wanninkhof (1998, A98) considers bubble mediated gas exchange and is used in simulation 8. The different parameterizations (LM86, W99, N00, H06) were available from the AIRSEA version of Pozzer et al. (2006). The

ACPD
15, 17553–17598, 2015

N00 parameterization was normalized to the Schmidt number of 600 as in the original publication by Nightingale et al. (2000), while 660 was used in Z13.

Two additional simulations were performed, with a different k_w-parameterization, used here only for DMS. These parameterizations have been derived from in-situ eddy covariance measurements and deviate from previously published parameterizations, because the transfer velocity does not increase at wind speeds higher than 11 m s^{-1} (Bell et al., 2013) or because a linear relationship to wind speed is suggested (Marandino et al., 2009). Both simulations cover the period of 2004–2013, since observations from this period were available for comparison. These two parameterization for k_w were added to the submodule code of AIRSEA (for equations see Table 4). The modification of the code included a parameterization based on results of the study from Bell et al. (2013, B13m) with a conservative approach, in which the N00 parameterization was used until the wind speed of 11 m s^{-1} and kept constant at higher wind speeds to account for the missing increase of k_w with increasing wind speed. Finally, the parameterization by Marandino et al. (2009, M09) was used in simulation 10 for the same period as B13m.

2.4 Observational data

Simulated atmospheric mixing ratios of the trace gases from PWC and PE are compared to observations from ship campaigns, aircraft campaigns and – if available – ground based time series stations.

Twenty-three aircraft campaigns providing halocarbon data are considered in order to create annual zonal mean climatologies of these trace gases. The combined data set ranges from 90° N to 75° S, transecting from the surface to the upper troposphere/lower stratosphere over land and ocean from 1992 to 2012 (see Table S1 for details on the aircraft campaigns). Many of the more recent data sets are inter-calibrated (see e.g. Brinckmann et al., 2012; Hall et al., 2014; Sala et al., 2014; Wisher et al., 2014). The latitudinal and longitudinal distributions and names of the aircraft campaigns are illustrated in Fig. 3a. The measurements were averaged in zonal 10° wide latitude bins with

ACPD
15, 17553–17598, 2015

a vertical extent ranging from 10 to 50 hPa (10 hPa in boundary layer and TTL region). Most of the measurements are located around 30° N of latitude with more than 150 points per bin. The tropical region (20° N–20° S) has an average of 50 points per bin. Figure S1 in the Supplement illustrates the numbers of the measurements per bin. For the comparison of measured and modelled data, the EMAC output of simulations 1 and 2 is first sampled at the same location of the aircraft measurements (longitude, latitude, altitude and time) by linear interpolation. Then, the same process of averaging per bin as for the measurements is applied to the model output.

Nine coastal ground stations from NOAA/ESRL, where halocarbons have been measured from the 1990ies on by the NOAA global flask sampling network, from the database HalOcAt (Ziska et al., 2013), were chosen for comparison due to their location close to the coast (Table 2). Two time series stations situated distant to the coast (Park Falls, Wisconsin, Niwot Ridge Forest, Colorado, both USA) were chosen to assess to contribution of marine halocarbon emissions to the atmospheric mixing ratio over land. Monthly means of the time series were compared to monthly means of simulation 1 and 2 for the PWC and PE set-up.

DMS was directly compared to measurements from ship campaigns in the marine boundary layer, because no data from ground based time series stations is available. Campaigns chosen were PHASE-I (2004, Marandino et al., 2007), 2 campaigns on RV *Knorr* (Marandino et al., 2007, 2008), and M98 on RV *Meteor* (2009, A. C. Zavarsky, personal communication, 2014) to ensure a broad spatial coverage (Fig. 3b). Upper air atmospheric concentrations were compared to air craft measurements from the HIAPER Pole-to-Pole observation (HIPPO) campaigns 1–5 (Wofsy et al., 2012), again subsampling the model output for time and location of the observations.

ACPD
15, 17553–17598, 2015

3 Results and discussion

3.1 Global emissions based on prescribed concentrations

The long-term mean of global emissions (1990–2013, simulation 1 in Table 1) based on PWC differ for the four gases tested and varies between +11 % ($CHBr_3$) to −28 % (CH_2Br_2) (Table 3), but yield globally a similar spatial pattern of emissions as Z13/L11 (Figs. 4 and 5). Although global emissions for CH_2Br_2 were reduced in the PWC set-up compared to the Z13 scenario, they still lie in the range of previously published estimates (61.8–112.7 $Tg\,yr^{-1}$, Table 3). The global PWC emissions for $CHBr_3$ are 11 % higher than that from Z13, but still 47–60 % lower than top-down approaches by Warwick et al. (2006), Liang et al. (2010) and Ordóñez et al. (2012). The PWC $CHBr_3$ emissions lie at the lower end of emission scenarios, closest to Z13. The same holds for CH_3I, where emissions are 2 % higher compared to Z13 but still 18 % lower than the published estimate from Bell et al. (2002). Emission estimates in PWC are closest to Z13 and thus at the lower end of the range of published global emission estimates. DMS emissions in PWC compared to L11 were 17 % lower (Table 3).

The main differences between the two approaches result from considering the actual state of the atmosphere when calculating emissions from PWC, since the atmospheric mixing ratio of the gas has a direct feedback on its emissions through the concentration gradient (Eq. 1). Higher atmospheric concentrations lead to lower marine emissions (or can even lead to deposition) and vice versa. In the PWC set-up where the actual concentration gradient between the ocean surface concentration and the model's atmospheric mixing ratio is considered, the emissions thus respond consistently to this feedback. The most obvious example for that is the global emission of DMS. In L11, an atmospheric concentration of 0 ppt is assumed justified by the high super saturation in the water and the short lifetime of DMS. In the PWC approach in our study, the atmospheric mixing ratio is always higher than 0 ppt, on average 133 (± 125) ppt, and this is likely the main reason for the resulting 17 % reduction in the modelled flux vs. L11 (Fig. 5).

ACPD
15, 17553–17598, 2015

Considering the actual state of the atmosphere leads to altered concentration gradients and thus emissions for any gas in the PWC set-up, but the impact on global emissions depends on the specific characteristics and global distribution of the gas in the surface ocean. For example, the impact of the PWC approach on global emissions for CH_2Br_2 (28 % difference between PWC and Z13) is larger than that for CH_3I (2 % difference) (Table 3). This difference can be explained by the saturation of the two gases: CH_3I is mainly oversaturated in the surface ocean with a mean saturation ratio (actual concentration divided by equilibrium concentration) of 18.2 in Z13. CH_2Br_2 with a mean saturation ratio of 2 is concentrated closer to equilibrium. The distance from equilibrium is thus larger for CH_3I than for CH_2Br_2. Changes in atmospheric mixing ratio therefore affect the concentration gradient for CH_2Br_2 more than for CH_3I. For $CHBr_3$ with a similar global ocean surface saturation ratio as CH_2Br_2, a drastic change in emissions between PWC and Z13 can be seen in the Southern Hemisphere (50–90° S Table 3), where the emissions increase two orders of magnitude in the PWC compared to Z13. The Z13 emission climatology displays a latitudinal band of elevated atmospheric mixing ratios around 60° S, which result in this region being a sink for atmospheric $CHBr_3$. In our PWC set-up, atmospheric mixing ratio in this region are not as elevated and hence PWC leads to larger emissions. In general, gases that are concentrated close to equilibrium in the surface ocean respond stronger to changes in atmospheric concentrations and thus to the PWC set-up than more supersaturated gases.

Comparing integrated regional fluxes, the halocarbons display the largest differences in the polar regions (Table 3). Besides dynamic atmospheric concentrations that may alter emissions in the PE set-up, two other reasons for differences in this specific set-up apply for the halocarbons. First, no sea ice is considered in Z13 whereas EMAC uses prescribed sea-ice in our PWC set-up. L11 considers sea-ice. When sea ice is present in the model EMAC/AIRSEA, the flux is reduced by the fraction of surface that is covered by it. This may lead to the lower flux estimations in our PWC set-up and may partly explain e.g. the reduced emissions in the Arctic for $CHBr_3$. Furthermore, our

ACPD
15, 17553–17598, 2015

PWC approach takes into account air-side transfer velocity (Eq. 2) instead of only the water-side transfer velocity as Z13, which can control the flux of more soluble gases at low temperatures and thus decrease emissions (McGillis et al., 2000). At high latitudes (60–90° N and S), where low temperatures and high winds prevail, the transfer velocity is reduced by 43 % (CH_2Br_2), 27 % ($CHBr_3$) and 6 % (CH_3I) using k_{air} in the PWC set-up. L11 takes the k_{air} and sea-ice into account, thus this difference does not apply.

3.2 Atmospheric mixing ratios based on PWC and PE

The atmospheric mixing ratios in EMAC sustained by emissions either from PWC or PE are compared to available atmospheric observations from aircraft campaigns (halocarbons, DMS), ground based time series stations from NOAA/ESRL (halocarbons) and ship campaigns (DMS). The model output of simulations 1 and 2 (Tables 1 and 4) was subsampled at the times and locations of the observations.

The largest difference between PWC and PE in the atmospheric mixing ratio is again found for CH_2Br_2 in the Southern Hemisphere (Fig. 6), where the PWC set-up yields lower emissions and therefore also lower atmospheric mixing ratios. For CH_2Br_2, atmospheric mixing ratios globally decrease on average by 28 % compared to the PE set-up, which is the same percentage as the reduction in the global emissions. Concentrations derived from these reduced fluxes generally agree better with the measurements, even though Arctic emissions still seem to be underestimated in the model compared to the observations. A possible explanation for this underestimation could be emissions of VSLS from sea ice that are not considered in the model, as e.g. Karlsson et al. (2013) observed elevated CH_2Br_2 in brines on top of sea ice. Mixing ratios of $CHBr_3$ are similar in the PWC and PE set-up (difference only 1.2 %), but both do not show the same pattern as the measurements: for both set-ups, atmospheric mixing ratios are underestimated in the Southern Hemisphere up to the northern tropics (Fig. 6). The same is evident for CH_3I, where PWC and PE also vary only slightly, while both set-ups underestimate atmospheric CH_3I concentration in the tropics. Since atmospheric concentrations were derived from emissions based on the Z13/L11 water concentration climatol-

ACPD
15, 17553–17598, 2015

ogy in the PWC set-up, negative discrepancies to atmospheric observations indicate regions where the concentration climatologies lack hotspots and can thus identify missing oceanic source regions. For all three halocarbons, the concentration climatologies seem to represent water concentrations that are too low in the Northern Hemisphere and the tropics to explain the observed atmospheric mixing ratios. It has to be noted that coastal areas are large source regions of halocarbon emissions with global contributions of up to 70 % (Ziska et al., 2013), which might be underrepresented in our modelled approach and thus might at least partly explain these missing sources.

Modelled concentrations matched observations from NOAA/ESRL ground stations in most of the cases better in the PWC set-up compared to PE. The agreement between simulation and measurements increases with the atmospheric lifetime of the gases: modelled mixing ratios for CH_2Br_2, with the longest lifetime of the tested gases, reflect the observed seasonality at all 12 stations well (Fig. 7). The modelled seasonality of the atmospheric mixing ratios is similar in both the PWC and PE set-ups, indicating that the main fluctuations at these locations comes from seasonality in atmospheric transport and chemistry rather than from seasonality in emissions, since emissions are constant in PE. For all stations except for Mace Head, PWC yields atmospheric mixing ratios closer to the measurements for CH_2Br_2, reducing overestimations of modelled atmospheric mixing ratios compared to measurements of up to 75 % as e.g. at the South Pole. Discrepancies between observations and model simulations are larger in most of the ground based stations for $CHBr_3$ (lifetime ~ 20 days in our simulation) than for CH_2Br_2, and again PWC yields equally well or more accurate mixing ratios than PE compared to the measurements (Fig. 8). However, the observed seasonality is not well reflected in both the PWC and the PE set-up. This mismatch indicates that a further seasonality in the sources is required, which can e.g. be accounted for by introducing a seasonality in the water concentrations prescribed. This finding is opposite to findings from Liang et al. (2010), who concluded that atmospheric $CHBr_3$ mixing ratios are mainly driven by transport and atmospheric chemistry. Furthermore, the good agreement between model and observations at continental sites away from

ACPD
15, 17553–17598, 2015

the coast (Park Falls, Wisconsin, USA, Niwot Ridge Forest, Colorado, USA) for CH_2Br_2 and $CHBr_3$ indicates that the ocean is the dominant source of these compounds also over land. CH_3I, the gas with the shortest lifetime in the range of a few days, shows the largest discrepancies between modeled mixing ratios and observations (Fig. 9). The PWC set-up yields mixing ratios in the range of the observations for only 2 stations (Alert, Canada and Barrow, Alaska, USA), and in most of the stations, the seasonality was not well reflected in the model runs. CH_3I seasonality in water concentrations has previously been observed (Shi et al., 2014), indicating that seasonally resolved water concentrations are needed to reproduce atmospheric concentrations of the shortest lived compounds in a more accurate way. Oceanic emissions in PE and PWC were too large to explain atmospheric mixing ratios at stations in high latitudes (Summit, Mace Head, Cape Grim, Palmer Station, South Pole), but too low to explain atmospheric mixing ratios in lower latitudes (Park Falls, Trinidad Head, Niwot Ridge, Cape Kumuhaki, Mauna Loa), which agrees with findings from aircraft campaigns (Fig. 6).

Four ship campaigns were chosen for comparison of DMS, since long-term measurements of atmospheric mixing ratios of DMS are not available. In addition, no observations from time series stations are available, which makes an analysis of seasonality as done for the halocarbons difficult. Simulation with both the PWC (N00) and the PE approach overestimate DMS mixing ratios in the marine boundary layer from ship campaigns (see positive Δ in Table 5) by 47.8 % (PE) and 23.35 % (PWC). However, the PWC reduces discrepancies within both ship and aircraft campaigns by a factor of 2 (Table 5).

An overall comparison of the agreement of both set-ups with observations is summarized in a Taylor-diagram (Fig. 10). This diagram is a statistical summary that shows how well two patterns match each other with regard to their correlation, variance and root-mean-square difference (Taylor, 2001). The closer a point of a specific set-up is located to the reference point of observations (here 1.0 on x axis), the more the simulation resembles the observed measurements. PWC simulations increased the agreement with observations for CH_2Br_2, especially the correlation (0.4 in PE to 0.6 in PWC),

ACPD
15, 17553–17598, 2015

and for DMS (0.53 in PE to 0.65 in PWC), but only very slightly for $CHBr_3$ and CH_3I. Atmospheric mixing ratios are thus reproduced slightly ($CHBr_3$, CH_3I) or much (CH_2Br_2, DMS) better in the PWC set-up compared to the PE set-up.

3.3 Comparison of different transfer velocity (k_w) parameterizations

A large uncertainty of global emission estimates is related to different parameterizations of the transfer velocity in Eq. (1). Calculating emissions online enables a simple way of testing different transfer velocity parameterizations, which was realized here with eight 2 year simulations described in Table 1 (simulations 3–10).

Largest sensitivity for the emissions of all gases is introduced by different parameterizations of the water-side transfer velocity k_w tested in simulations 3–6 (Table 4). The 4 parameterizations that were tested (simulation 3–6, Table 1) comprised linear (LM86, simulation 3), cubic (W99, simulation 4) and quadratic (N00, simulation 5, H06, simulation 6) relations to wind speed. The resulting global emission estimates in these parameterizations range between 53.7 to 65.1 $Gg\,yr^{-1}$ for CH_2Br_2, 189.0 to 249.7 $Gg\,yr^{-1}$ for $CHBr_3$, 151.9 to 225.7 $Gg\,yr^{-1}$ for CH_3I and 33.4 to 48.7 $Tg\,yr^{-1}$ for DMS (Table 4). As expected, the linear k_w-parameterization (LM86) yields the lowest global emission estimates, since it produces the lowest k_w values (Fig. 2). The N00 parameterization produces highest global fluxes for $CHBr_3$ and CH_2Br_2, but not for DMS and CH_3I, where the highest fluxes were obtained by H06 (DMS) and W99 (CH_3I) (Table 4). The fact that different parameterizations lead to highest global estimates for different gases is explained by the varying spatial distribution of concentration hot spots and regional variations of wind.

The k_w parameterization adding flux under calm conditions due to precipitation (simulation 7 in Table 4) resulted in a 4 % (CH_2Br_2) to 6 % (DMS) additional flux (Table 4) to the atmosphere for all the compounds compared to the reference flux using H06 alone (simulation 6, Table 4). Additional flux due to precipitation is inversely correlated to the Schmidt number, so that under identical conditions, increasing flux would be added in the order $CHBr_3 > CH_2Br_2 > DMS > CH_3I$. The global flux estimations compared to the

ACPD
15, 17553–17598, 2015

reference run do not increase in this order (Table 4), but DMS > $CHBr_3$/CH_3I > CH_2Br_2. This non-uniform response among the gases is explained by the globally and regionally varying distance from equilibrium for the four gases, which together with regional precipitation patterns leads to variations in the emissions increased by rain. White cap coverage as an own parameterization according to A98 also has small but ambivalent effects on the global flux for the different compounds (simulation 8, Table 4). Compared to the mean of all nonlinear parameterizations for each gas, global emissions were higher when the white cap coverage parameterization was used for $CHBr_3$ (4 %) and CH_2Br_2 (2 %) but lower for CH_3I (−8 %) and DMS (−6 %) (Table 4).

The parameterizations tested only for DMS are both derived from eddy covariance measurements at sea. Both parameterizations reduced the global emissions by 4.4 % (B13m) and 1.2 % (M09) compared to the average flux of simulation 3–6 (Table 4). Although the modelled atmospheric mixing ratios at the time and location of observations is for both of the parameterizations higher than the observations, discrepancies between simulated and observed mixing ratios were reduced compared to the N00 parameterization by a factor of 1.4 (B13m) and 1.2 (M09).

4 Summary and conclusions

Two different ways of considering marine emissions of trace gases in global atmospheric chemistry models are discussed here for the halocarbons CH_2Br_2, $CHBr_3$, CH_3I and the sulfur containing compound DMS. In contrast to prescribing emissions (PE) from oceanic and atmospheric concentration climatologies in the model, prescribing water concentrations (PWC) with an online calculation of emissions results in a consistent concentration gradient between ocean and atmosphere. Marine emissions are thus modelled more consistently, as the concentration gradient that determines the direction and the magnitude of the emissions is in agreement with the modelled atmospheric boundary layer mixing ratio and the prescribed ocean surface concentration of the gas. The approach of modelling emissions online was successfully applied for the

ACPD
15, 17553–17598, 2015

very short-lived halocarbons for the first time and was based on the submodel AIRSEA coupled to EMAC by Pozzer et al. (2006). The method has a number of conceptual and practical advantages, as in this framework the modelled flux can respond in a consistent way to changes in sea surface temperature, surface wind speed, possible sea ice cover and marine atmospheric mixing ratios in the model.

Global emission estimates of the four gases differ between +11 % ($CHBr_3$) and −28 % (CH_2Br_2) between PWC and PE, when the transfer velocity k_w is parametrized according to Nightingale et al. (2000) in both set-ups. Prescribing water concentrations instead of emissions has the strongest effect for gases close to equilibrium in the surface ocean such as CH_2Br_2 (28 % reduced emissions in PWC compared to PE), as its emissions are most sensitive to atmospheric concentrations. In contrast, only 2 % difference is found for the highly supersaturated gas CH_3I. Considering PWC reduces the global emissions of DMS by 17 %. Comparison to observations revealed that PWC compared to PE reproduces observations slightly ($CHBr_3$, CH_3I) or much (CH_2Br_2, DMS) better for measurements made at ground based time series stations, aircraft campaigns and ship cruises. Even though it is clear that more data for all compounds are needed globally, the PWC set-up can be used to identify oceanic regions where more measurements will be needed to improve the global emission estimate. For example, there are clear discrepancies in the Northern Hemisphere for $CHBr_3$ and the tropics for CH_3I.

Global emission estimates display a large sensitivity towards the parameterization of the transfer velocity k_w, with uncertainties between 15.6 % (CH_2Br_2) and 35.9 % (CH_3I) compared to the mean global emissions of the four tested simulations including k_w parameterizations according to Liss and Merlivat (1986, LM86), Wanninkhof and McGillis (1999, W99), Nightingale et al. (2000, N00) and Ho et al. (2006, H06). Sensitivity towards rain or bubble mediated transfer was generally low (< 10 % change in global emission estimate). Two parameterization adapting results that have recently been suggested for DMS (Marandino et al., 2009, M09; Bell et al., 2013, B13m) produced both a lower global emission estimate, which at the same time reduced discrepancies

ACPD
15, 17553–17598, 2015

between simulated and observed atmospheric mixing ratios and yielded simulated atmospheric mixing ratios closer to observations than simulated mixing ratios with the N00 parameterization.

In summary, prescribing water concentrations instead of prescribing emissions in global atmospheric chemistry models leads to a consistent concentration gradient between ocean and atmosphere on one hand, and enables convenient testing of different air–sea gas exchange parameterizations on the other hand. Based on the results of our comparison between the PE and PWC, prescribing concentrations leads to more consistent emissions and mainly more accurate reproduction of observations of atmospheric mixing ratios of the VSLS described here.

The Supplement related to this article is available online at doi:10.5194/acpd-15-17553-2015-supplement.

Acknowledgements. This work was supported through the German Federal Ministry of Education and Research through the project ROMIC-THREAT (BMBF-FK01LG1217A). Additional funding for C. Marandino and S. Lennartz came from the Helmholtz Young Investigator Group of C. Marandino, TRASE-EC (VH-NG-819), from the Helmholtz Association through the President's Initiative and Networking Fund and the GEOMAR Helmholtz-Zentrum für Ozeanforschung Kiel. We thank A. Pozzer for advice on the use of AIRSEA and valuable comments on the manuscript. Thanks to D. R. Blake from the University of California, Irvine for advice and the data access. Thanks to A. Lana for providing emission and concentration fields of DMS and to A. C. Zavarsky for atmospheric DMS measurements on the Meteor 98 cruise. We thank Prabir Patra for his help and for providing the OH field used in the EMAC simulations. NOAA measurements were supported in part by NOAA's Atmospheric Chemistry, Carbon Cycle and Climate Program of its Climate program Office. Data on halocarbon mixing ratios from aircraft campaigns were obtained from the ESPO NASA archive and from the EOL-NCAR database. We would like to acknowledge operational, technical and scientific support provided by NCAR's Earth Observing Laboratory, sponsored by the National Science Foundation. University Frank-

furt would like to thank DLR for organizing and funding the ESMVal campaign and DFG (grant. No. 367/8 and EN367/11) for funding the TACTS campaign and the measurements.

References

Aschmann, J., Sinnhuber, B.-M., Atlas, E. L., and Schauffler, S. M.: Modeling the transport of very short-lived substances into the tropical upper troposphere and lower stratosphere, Atmos. Chem. Phys., 9, 9237–9247, doi:10.5194/acp-9-9237-2009, 2009.

Asher, W. E. and Wanninkhof, R.: The effect of bubble-mediated gas transfer on purposeful dual-gaseous tracer experiments, J. Geophys. Res.-Oceans, 103, 10555–10560, doi:10.1029/98jc00245, 1998.

Bates, T. S., Lamb, B. K., Guenther, A., Dignon, J., and Stoiber, R. E.: Sulfur emissions to the atmosphere from natural sources, J. Atmos. Chem., 14, 315–337, doi:10.1007/bf00115242, 1992.

Bell, N., Hsu, L., Jacob, D. J., Schultz, M. G., Blake, D. R., Butler, J. H., King, D. B., Lobert, J. M., and Maier-Reimer, E.: Methyl iodide: atmospheric budget and use as a tracer of marine convection in global models, J. Geophys. Res.-Atmos., 107, 4340, doi:10.1029/2001jd001151, 2002.

Bell, T. G., De Bruyn, W., Miller, S. D., Ward, B., Christensen, K. H., and Saltzman, E. S.: Air-sea dimethylsulfide (DMS) gas transfer in the North Atlantic: evidence for limited interfacial gas exchange at high wind speed, Atmos. Chem. Phys., 13, 11073–11087, doi:10.5194/acp-13-11073-2013, 2013.

Brinckmann, S., Engel, A., Bönisch, H., Quack, B., and Atlas, E.: Short-lived brominated hydrocarbons – observations in the source regions and the tropical tropopause layer, Atmos. Chem. Phys., 12, 1213–1228, doi:10.5194/acp-12-1213-2012, 2012.

Chameides, W. L. and Davis, D. D.: Iodine – its possible role in tropospheric photochemistry, J. Geophys. Res.-Oc. Atm., 85, 7383–7398, doi:10.1029/JC085iC12p07383, 1980.

Charlson, R. J., Lovelock, J. E., Andreae, M. O., and Warren, S. G.: Oceanic phytoplankton, atmospheric sulfur, cloud albedo and climate, Nature, 326, 655–661, doi:10.1038/326655a0, 1987.

De Bruyn, W. J., Swartz, E., Hu, J. H., Shorter, J. A., Davidovits, P., Worsnop, D. R., Zahniser, M. S., and Kolb, C. E.: Henrys law solubilities and setcheniw coefficients for biogenic

reduced sulphur species obtained from gas-liquid uptake measurements, J. Geophys. Res.-Atmos., 100, 7245–7251, doi:10.1029/95JD00217, 1995.

Dee, D. P., Uppala, S. M., Simmons, A. J., Berrisford, P., Poli, P., Kobayashi, S., Andrae, U., Balmaseda, M. A., Balsamo, G., Bauer, P., Bechtold, P., Beljaars, A. C. M., van de Berg, L., Bidlot, J., Bormann, N., Delsol, C., Dragani, R., Fuentes, M., Geer, A. J., Haimberger, L., Healy, S. B., Hersbach, H., Hólm, E. V., Isaksen, L., Kållberg, P., Köhler, M., Matricardi, M., McNally, A. P., Monge-Sanz, B. M., Morcrette, J. J., Park, B. K., Peubey, C., de Rosnay, P., Tavolato, C., Thépaut, J. N., and Vitart, F.: The era-interim reanalysis: configuration and performance of the data assimilation system, Q. J. Roy. Meteor. Soc., 137, 553–597, doi:10.1002/qj.828, 2011.

Hall, B. D., Engel, A., Mühle, J., Elkins, J. W., Artuso, F., Atlas, E., Aydin, M., Blake, D., Brunke, E.-G., Chiavarini, S., Fraser, P. J., Happell, J., Krummel, P. B., Levin, I., Loewenstein, M., Maione, M., Montzka, S. A., O'Doherty, S., Reimann, S., Rhoderick, G., Saltzman, E. S., Scheel, H. E., Steele, L. P., Vollmer, M. K., Weiss, R. F., Worthy, D., and Yokouchi, Y.: Results from the International Halocarbons in Air Comparison Experiment (IHALACE), Atmos. Meas. Tech., 7, 469–490, doi:10.5194/amt-7-469-2014, 2014.

Hayduk, W. and Laudie, H.: Prediction of diffusion coefficients for nonelectrolytes in dilute aqueous solutions, AICHE J., 20, 611–615, doi:10.1002/aic.690200329, 1974.

Hepach, H., Quack, B., Raimund, S., Fischer, T., Atlas, E. L., and Bracher, A.: Halocarbon emissions and sources in the equatorial Atlantic Cold Tongue, Biogeosciences Discuss., 12, 5559–5608, doi:10.5194/bgd-12-5559-2015, 2015.

Ho, D. T., Zappa, C. J., McGillis, W. R., Bliven, L. F., Ward, B., Dacey, J. W. H., Schlosser, P., and Hendricks, M. B.: Influence of rain on air–sea gas exchange: lessons from a model ocean, J. Geophys. Res.-Oceans, 109, C08S18, doi:10.1029/2003jc001806, 2004.

Ho, D. T., Law, C. S., Smith, M. J., Schlosser, P., Harvey, M., and Hill, P.: Measurements of air–sea gas exchange at high wind speeds in the southern ocean: implications for global parameterizations, Geophys. Res. Lett., 33, L16611, doi:10.1029/2006gl026817, 2006.

Hopkins, F. E. and Archer, S. D.: Consistent increase in dimethyl sulfide (DMS) in response to high CO_2 in five shipboard bioassays from contrasting NW European waters, Biogeosciences, 11, 4925–4940, doi:10.5194/bg-11-4925-2014, 2014.

Hossaini, R., Chipperfield, M. P., Monge-Sanz, B. M., Richards, N. A. D., Atlas, E., and Blake, D. R.: Bromoform and dibromomethane in the tropics: a 3-D model study of chemistry and transport, Atmos. Chem. Phys., 10, 719–735, doi:10.5194/acp-10-719-2010, 2010.

ACPD
15, 17553–17598, 2015

Hossaini, R., Mantle, H., Chipperfield, M. P., Montzka, S. A., Hamer, P., Ziska, F., Quack, B., Krüger, K., Tegtmeier, S., Atlas, E., Sala, S., Engel, A., Bönisch, H., Keber, T., Oram, D., Mills, G., Ordóñez, C., Saiz-Lopez, A., Warwick, N., Liang, Q., Feng, W., Moore, F., Miller, B. R., Marécal, V., Richards, N. A. D., Dorf, M., and Pfeilsticker, K.: Evaluating global emission inventories of biogenic bromocarbons, Atmos. Chem. Phys., 13, 11819–11838, doi:10.5194/acp-13-11819-2013, 2013.

Hossaini, R., Chipperfield, M. P., Montzka, S. A., Rap, A., Dhomse, S., and Feng, W.: Efficiency of short-lived halogens at influencing climate through depletion of stratospheric ozone, Nat. Geosci, 8., 186–190, doi:10.1038/ngeo2363, 2015.

Jöckel, P.: Technical note: Recursive rediscretisation of geo-scientific data in the Modular Earth Submodel System (MESSy), Atmos. Chem. Phys., 6, 3557–3562, doi:10.5194/acp-6-3557-2006, 2006.

Jöckel, P., Tost, H., Pozzer, A., Brühl, C., Buchholz, J., Ganzeveld, L., Hoor, P., Kerkweg, A., Lawrence, M. G., Sander, R., Steil, B., Stiller, G., Tanarhte, M., Taraborrelli, D., van Aardenne, J., and Lelieveld, J.: The atmospheric chemistry general circulation model ECHAM5/MESSy1: consistent simulation of ozone from the surface to the mesosphere, Atmos. Chem. Phys., 6, 5067–5104, doi:10.5194/acp-6-5067-2006, 2006.

Jöckel, P., Kerkweg, A., Pozzer, A., Sander, R., Tost, H., Riede, H., Baumgaertner, A., Gromov, S., and Kern, B.: Development cycle 2 of the Modular Earth Submodel System (MESSy2), Geosci. Model Dev., 3, 717–752, doi:10.5194/gmd-3-717-2010, 2010.

Karlsson, A., Theorin, M., and Abrahamsson, K.: Distribution, transport, and production of volatile halocarbons in the upper waters of the ice-covered high arctic ocean, Global Biogeochem. Cy., 27, 1246–1261, doi:10.1002/2012gb004519, 2013.

Kerkweg, A., Buchholz, J., Ganzeveld, L., Pozzer, A., Tost, H., and Jöckel, P.: Technical Note: An implementation of the dry removal processes DRY DEPosition and SEDImentation in the Modular Earth Submodel System (MESSy), Atmos. Chem. Phys., 6, 4617–4632, doi:10.5194/acp-6-4617-2006, 2006a.

Kerkweg, A., Sander, R., Tost, H., and Jöckel, P.: Technical note: Implementation of prescribed (OFFLEM), calculated (ONLEM), and pseudo-emissions (TNUDGE) of chemical species in the Modular Earth Submodel System (MESSy), Atmos. Chem. Phys., 6, 3603–3609, doi:10.5194/acp-6-3603-2006, 2006b.

Kondo, J.: Air-sea bulk transfer coefficients in diabatic conditions, Bound.-Lay. Meteorol., 9, 91–112, doi:10.1007/bf00232256, 1975.

ACPD
15, 17553–17598, 2015

Lana, A., Bell, T. G., Simo, R., Vallina, S. M., Ballabrera-Poy, J., Kettle, A. J., Dachs, J., Bopp, L., Saltzman, E. S., Stefels, J., Johnson, J. E., and Liss, P. S.: An updated climatology of surface dimethlysulfide concentrations and emission fluxes in the global ocean, Global Biogeochem. Cy., 25, GB1004, doi:10.1029/2010gb003850, 2011.

Liang, Q., Stolarski, R. S., Kawa, S. R., Nielsen, J. E., Douglass, A. R., Rodriguez, J. M., Blake, D. R., Atlas, E. L., and Ott, L. E.: Finding the missing stratospheric Br_y: a global modeling study of $CHBr_3$ and CH_2Br_2, Atmos. Chem. Phys., 10, 2269–2286, doi:10.5194/acp-10-2269-2010, 2010.

Lin, S. J. and Rood, R. B.: Multidimensional flux-form semi-lagrangian transport schemes, Mon. Weather Rev., 124, 2046–2070, doi:10.1175/1520-0493(1996)124<2046:MFFSLT>2.0.CO;2, 1996.

Liss, P. S. and Merlivat, L.: Air-sea gas exchange rates: introduction and synthesis, in: The Role of Air-sea Gas Exchange in Geochemical Cycling, edited by: Buat-Menard, P. and Reidel, D., Norwell, Mass., 113–127, 1986.

Liss, P. S. and Slater, P.: Flux of gases across the air–sea interface, Nature, 247, 181–184, 1974.

Lovelock, J. E. and Maggs, R. J.: Halogenated hydrocarbons in and over the atlantic, Nature, 241, 194–196, doi:10.1038/241194a0, 1973.

Lyman, W., Reehl, W., and Rosenblatt, D.: Handbook of Chemical Property Estimation Mehods, American Chemical Society, Washington DC, USA, 1990.

Marandino, C. A., De Bruyn, W. J., Miller, S. D., and Saltzman, E. S.: Eddy correlation measurements of the air/sea flux of dimethylsulfide over the north pacific ocean, J. Geophys. Res.-Atmos., 112, D03301, doi:10.1029/2006jd007293, 2007.

Marandino, C. A., De Bruyn, W. J., Miller, S. D., and Saltzman, E. S.: DMS air/sea flux and gas transfer coefficients from the north atlantic summertime coccolithophore bloom, Geophys. Res. Lett., 35, L23812, doi:10.1029/2008gl036370, 2008.

Marandino, C. A., De Bruyn, W. J., Miller, S. D., and Saltzman, E. S.: Open ocean DMS air/sea fluxes over the eastern South Pacific Ocean, Atmos. Chem. Phys., 9, 345–356, doi:10.5194/acp-9-345-2009, 2009.

Marandino, C. A., Tegtmeier, S., Krüger, K., Zindler, C., Atlas, E. L., Moore, F., and Bange, H. W.: Dimethylsulphide (DMS) emissions from the western Pacific Ocean: a potential marine source for stratospheric sulphur?, Atmos. Chem. Phys., 13, 8427–8437, doi:10.5194/acp-13-8427-2013, 2013a.

Marandino, C. A., Tegtmeier, S., Krüger, K., Zindler, C., Atlas, E. L., Moore, F., and Bange, H. W.: Corrigendum to "Dimethylsulphide (DMS) emissionsfrom the West Pacific Ocean: a potential marine source for stratospheric sulphur?" published in Atmos. Chem. Phys., 13, 8427–8437, 2013, Atmos. Chem. Phys., 13, 8813–8814, doi:10.5194/acp-13-8813-2013, 2013b.

McGillis, W. R., Dacey, J. W. H., Frew, N. M., Bock, E. J., and Nelson, R. K.: Water-air flux of dimethylsulfide, J. Geophys. Res.-Oceans, 105, 1187–1193, doi:10.1029/1999jc900243, 2000.

Montzka, S. A., Reimann, S., Engel, A., Krüger, K., O'Doherty, S., and Sturges, W. T.: Ozone-Depleting Substances (ODSs) and Related Chemicals, Scientific Assessment of Ozone Depletion: 2010, Global Ozone Research and Monitoring Project-Report No. 52. World Meteorological Organization, Geneva, Switzerland, 112 pp., 2011.

Moore, R. M., Geen, C. E., and Tait, V. K.: Determination of henry law constants for a suite of naturally-occurring halogenated methanes in seawater, Chemosphere, 30, 1183–1191, doi:10.1016/0045-6535(95)00009-w, 1995.

Nightingale, P. D., Malin, G., Law, C. S., Watson, A. J., Liss, P. S., Liddicoat, M. I., Boutin, J., and Upstill-Goddard, R. C.: In situ evaluation of air–sea gas exchange parameterizations using novel conservative and volatile tracers, Global Biogeochem. Cy., 14, 373–387, doi:10.1029/1999gb900091, 2000.

Notholt, J. and Bingemer, H.: Precursor gas measurements, chapter 2, in: The Sparc Asessment of Stratospheric Aerosol Particles, edited by: Thomason, L. W. and Peter, Th., WCRP-129, WMO/TD-No.1295, SPARC Report, 29–76, 2006.

Ordóñez, C., Lamarque, J.-F., Tilmes, S., Kinnison, D. E., Atlas, E. L., Blake, D. R., Sousa Santos, G., Brasseur, G., and Saiz-Lopez, A.: Bromine and iodine chemistry in a global chemistry-climate model: description and evaluation of very short-lived oceanic sources, Atmos. Chem. Phys., 12, 1423–1447, doi:10.5194/acp-12-1423-2012, 2012.

Orkin, V. L., Khamaganov, V. G., Kozlov, S. N., and Kurylo, M. J.: Measurements of rate constants for the oh reactions with bromoform ($CHBr_3$), $CHBr_2Cl$, $CHBrCl_2$, and epichlorohydrin (C_3H_5ClO), J. Phys. Chem.-US, 117, 3809–3818, doi:10.1021/jp3128753, 2013.

Papanastasiou, D. K., McKeen, S. A., and Burkholder, J. B.: The very short-lived ozone depleting substance $CHBr_3$ (bromoform): revised UV absorption spectrum, atmospheric lifetime and ozone depletion potential, Atmos. Chem. Phys., 14, 3017–3025, doi:10.5194/acp-14-3017-2014, 2014.

Patra, P. K., Krol, M. C., Montzka, S. A., Arnold, T., Atlas, E. L., Lintner, B. R., Stephens, B. B., Xiang, B., Elkins, J. W., Fraser, P. J., Ghosh, A., Hintsa, E. J., Hurst, D. F., Ishijima, K., Krummel, P. B., Miller, B. R., Miyazaki, K., Moore, F. L., Muehle, J., O'Doherty, S., Prinn, R. G., Steele, L. P., Takigawa, M., Wang, H. J., Weiss, R. F., Wofsy, S. C., and Young, D.: Observational evidence for interhemispheric hydroxyl-radical parity, Nature, 513, 219–223, doi:10.1038/nature13721, 2014.

Penkett, S. A., Jones, B. M. R., Rycroft, M. J., and Simmons, D. A.: An interhemispheric comparison of the concentrations of bromine compounds in the atmosphere, Nature, 318, 550–553, doi:10.1038/318550a0, 1985.

Pozzer, A., Jöckel, P., Sander, R., Williams, J., Ganzeveld, L., and Lelieveld, J.: Technical Note: The MESSy-submodel AIRSEA calculating the air–sea exchange of chemical species, Atmos. Chem. Phys., 6, 5435–5444, doi:10.5194/acp-6-5435-2006, 2006.

Quack, B. and Wallace, D. W. R.: Air-sea flux of bromoform: controls, rates, and implications, Global Biogeochem. Cy., 17, 1023, doi:10.1029/2002gb001890, 2003.

Saiz-Lopez, A., Plane, J. M. C., Baker, A. R., Carpenter, L. J., von Glasow, R., Martin, J. C. G., McFiggans, G., and Saunders, R. W.: Atmospheric chemistry of iodine, Chem. Rev., 112, 1773–1804, doi:10.1021/cr200029u, 2012.

Sala, S., Bönisch, H., Keber, T., Oram, D. E., Mills, G., and Engel, A.: Deriving an atmospheric budget of total organic bromine using airborne in situ measurements from the western Pacific area during SHIVA, Atmos. Chem. Phys., 14, 6903–6923, doi:10.5194/acp-14-6903-2014, 2014.

Salawitch, R. J.: Atmospheric chemistry: biogenic bromine, Nature, 439, 275–277, doi:10.1038/439275a, 2006.

Salawitch, R. J., Weisenstein, D. K., Kovalenko, L. J., Sioris, C. E., Wennberg, P. O., Chance, K., Ko, M. K. W., and McLinden, C. A.: Sensitivity of ozone to bromine in the lower stratosphere, Geophys. Res. Lett., 32, L05811, doi:10.1029/2004gl021504, 2005.

Saltzman, E. S., King, D. B., Holmen, K., and Leck, C.: Experimental determination of the diffusion coefficient of dimethylsulfide in water, J. Geophys. Res.-Oceans, 98, 16481–16486, doi:10.1029/93jc01858, 1993.

Sander, R., Baumgaertner, A., Gromov, S., Harder, H., Jöckel, P., Kerkweg, A., Kubistin, D., Regelin, E., Riede, H., Sandu, A., Taraborrelli, D., Tost, H., and Xie, Z.-Q.: The atmospheric chemistry box model CAABA/MECCA-3.0, Geosci. Model Dev., 4, 373–380, doi:10.5194/gmd-4-373-2011, 2011.

ACPD
15, 17553–17598, 2015

Sheng, J.-X., Weisenstein, D. K., Luo, B.-P., Rozanov, E., Stenke, A., Anet, J., Bingemer, H., and Peter, T.: Global atmospheric sulfur budget under volcanically quiescent conditions: aerosol-chemistry-climate model predictions and validation, J. Geophys. Res.-Atmos., 120, 256–276, doi:10.1002/2014jd021985, 2015.

Shi, Q., Petrick, G., Quack, B., Marandino, C., and Wallace, D.: Seasonal variability of methyl iodide in the kiel fjord, J. Geophys. Res.-Oceans, 119, 1609–1620, doi:10.1002/2013jc009328, 2014.

Sinnhuber, B.-M., Sheode, N., Sinnhuber, M., Chipperfield, M. P., and Feng, W.: The contribution of anthropogenic bromine emissions to past stratospheric ozone trends: a modelling study, Atmos. Chem. Phys., 9, 2863–2871, doi:10.5194/acp-9-2863-2009, 2009.

Solomon, S., Garcia, R. R., and Ravishankara, A. R.: On the role of iodine in ozone depletion, J. Geophys. Res.-Atmos., 99, 20491–20499, doi:10.1029/94jd02028, 1994.

Taylor, K. E.: Summarizing multiple aspects of model performance in a single diagram, J. Geophys. Res.-Atmos., 106, 7183–7192, doi:10.1029/2000jd900719, 2001.

Tegtmeier, S., Krüger, K., Quack, B., Atlas, E., Blake, D. R., Boenisch, H., Engel, A., Hepach, H., Hossaini, R., Navarro, M. A., Raimund, S., Sala, S., Shi, Q., and Ziska, F.: The contribution of oceanic methyl iodide to stratospheric iodine, Atmos. Chem. Phys., 13, 11869–11886, doi:10.5194/acp-13-11869-2013, 2013.

Tiedtke, M.: A comprehensive mass flux scheme for cumulus parameterization in large-scale models, Mon. Weather Rev., 117, 1779–1800, doi:10.1175/1520-0493, 1989.

von Glasow, R., von Kuhlmann, R., Lawrence, M. G., Platt, U., and Crutzen, P. J.: Impact of reactive bromine chemistry in the troposphere, Atmos. Chem. Phys., 4, 2481–2497, doi:10.5194/acp-4-2481-2004, 2004.

Wanninkhof, R.: Relationship between wind speed and gas exchange over the ocean, J. Geophys. Res., 97, 7373–7382, 1992.

Wanninkhof, R. and McGillis, W. R.: A cubic relationship between air–sea CO_2 exchange and wind speed, Geophys. Res. Lett., 26, 1889–1892, doi:10.1029/1999gl900363, 1999.

Wanninkhof, R., Asher, W. E., Ho, D. T., Sweeney, C., and McGillis, W. R.: Advances in quantifying air–sea gas exchange and environmental forcing, Annual Review of Marine Science, 1, 213–244, doi:10.1146/annurev.marine.010908.163742, 2009.

Warwick, N. J., Pyle, J. A., Carver, G. D., Yang, X., Savage, N. H., O'Connor, F. M., and Cox, R. A.: Global modeling of biogenic bromocarbons, J. Geophys. Res.-Atmos., 111, D24305, doi:10.1029/2006jd007264, 2006.

ACPD
15, 17553–17598, 2015

Watts, S. F.: The mass budgets of carbonyl sulfide, dimethyl sulfide, carbon disulfide and hydrogen sulfide, Atmos. Environ., 34, 761–779, doi:10.1016/s1352-2310(99)00342-8, 2000.

Wilke, C. R. and Chang, P.: Some measurements of diffusion in liquids, J. Phys. Chem., 59, 5, doi:10.1016/0167-2789(95)00183-5, 1955.

Wisher, A., Oram, D. E., Laube, J. C., Mills, G. P., van Velthoven, P., Zahn, A., and Brenninkmeijer, C. A. M.: Very short-lived bromomethanes measured by the CARIBIC observatory over the North Atlantic, Africa and Southeast Asia during 2009–2013, Atmos. Chem. Phys., 14, 3557–3570, doi:10.5194/acp-14-3557-2014, 2014.

Wofsy, S. C., B. C. Daube, R. Jimenez, Kort, E., Pittman, J. V., Park, S., Commane, R., Xiang, B., Santoni, G., Jacob, D., Fisher, J., Pickett-Heaps, C., Wang, H., Wecht, K., Wang, Q.-Q., Stephens, B., Shertz, S., Watt, A. S., Romashkin, P., Campos, T., Haggerty, J., Cooper, W. A., Rogers, D., Beaton, S., Hendershot, R., Elkins, J. W., Fahey, D. W., Gao, R. S., Moore, F., Montzka, S. A., Schwarz, J. P., Perring, A. E., Hurst, D., Miller, B. R., Sweeney, C., Oltmans, S., Nance, D., Hintsa, E., Dutton, G., Watts, L. A., Spackman, J. R., Rosenlof, K. H., Ray, E. A., Hall, B., Zondlo, M. A., Diao, M., Keeling, R., Bent, J., Atlas, E. L., Lueb, R., and Mahoney, M. J.: Hippo combined discrete flask and gc sample ghg, halo-, hydrocarbon data (r_20121129), Center, C. d. I. A., Oak Ridge National Laboratory, Oak Ridge, Tenessee, USA, 2012.

Ziska, F., Quack, B., Abrahamsson, K., Archer, S. D., Atlas, E., Bell, T., Butler, J. H., Carpenter, L. J., Jones, C. E., Harris, N. R. P., Hepach, H., Heumann, K. G., Hughes, C., Kuss, J., Krüger, K., Liss, P., Moore, R. M., Orlikowska, A., Raimund, S., Reeves, C. E., Reifenhäuser, W., Robinson, A. D., Schall, C., Tanhua, T., Tegtmeier, S., Turner, S., Wang, L., Wallace, D., Williams, J., Yamamoto, H., Yvon-Lewis, S., and Yokouchi, Y.: Global sea-to-air flux climatology for bromoform, dibromomethane and methyl iodide, Atmos. Chem. Phys., 13, 8915–8934, doi:10.5194/acp-13-8915-2013, 2013.

ACPD
15, 17553–17598, 2015

Table 1. Set-up of model simulations evaluated in this study. PWC = prescribed water concentration, PE = prescribed emissions, AIRSEA = submodel for online calculation of emissions, OFFLEM = submodel for prescribing emissions. WCC = white cap coverage effect.

	Abbrev.	k_w-Parameterization	Emission calculation, submodule	Rain effect	WCC	Period
1	PWC	Nightingale (2000)	PWC, AIRSEA	No	No	1990–2013
2	PE	Prescribed emissions, no online calculation, k_w in original publications N00	PE, OFFLEM	No	No	1990–2013
3	LM86	Liss and Merlivat (1986)	PWC, AIRSEA	No	No	2010–2011
4	W99	Wanninkhof et al. (1999)	PWC, AIRSEA	No	No	2010–2011
5	N00	Nightingale (2000)	PWC, AIRSEA	No	No	2010–2011
6	H06	Ho et al. (2006)	PWC, AIRSEA	No	No	2010–2011
7	H06r	Ho et al. (2006)	PWC, AIRSEA	Yes	No	2010–2011
8	H06w	Ho et al. (2006)	PWC, AIRSEA	No	Yes	2010–2011
9	B13 m	Bell et al. (2013) modified, only DMS	PWC, AIRSEA	No	No	2004–2013
10	M09	Marandino et al. (2009)	PWC, AIRSEA	No	No	2004–2013

ACPD
15, 17553–17598, 2015

Table 2. Metadata of the ground based time series stations of NOAA considered in this study.

No.	Abbr.	Station Name	Latitude	Longitude	Elevation [m]	Period
1	ALT	Alert, Canada	82.45° N	62.51° W	210	1992–2011
2	SUM	Summit, Greenland	72.58° N	38.48° W	3209	2004–2011
3	BRW	Barrow, Alaska	71.32° N	156.61° W	27	1993–2011
4	MHD	Mace Head, Ireland	53.33° N	9.90° W	42	1998–2011
5	LEF	Park Falls, Wisconsin	45.95° N	90.27° W	868	1996–2011
6	THD	Trinidad Head, California	41.05° N	124.151° W	120	2002–2011
7	NWF	Niwot Ridge Forest, Colorado	40.03° N	105.55° W	3475	1993–2011
8	KUM	Cape Kumuhaki, Hawaii	8.72° N	167.72° E	39	1995–2011
9	MLF	Mauna Loa, Hawaii	19.53° N	155.58° W	3433	1993–2011
10	CGO	Cape Grim, Tasmania	40.68° S	144.69° E	164	1993–2011
11	PSA	Palmer Station, Antarctica	64.92° S	64.00° W	15	1997–2011
12	SPO	South Pole	90.00° S	59.00° E	2837	1993–2011

ACPD
15, 17553–17598, 2015

Table 3. Integrated global fluxes from this study (PWC: prescribed water concentrations, N00: k_w-parameterization of Nightingale et al., 2000) compared to previously published emission estimates. Note that Ziska et al. (2013) is a bottom-up approach and the water concentrations were used in the online flux calculations for the halocarbons; Lana et al. (2011) DMS water concentrations were used for DMS online calculations. Ordonez et al. (2012) Liang et al. (2010) and Warwick et al. (2006) are top-down approaches, Bell et al. (2002) is a oceanic mixed-layer bottom-up model approach for CH_3I. Results form this study are indicated in bold letters.

	CH_2Br_2 ($Ggyr^{-1}$)					$CHBr_3$ ($Ggyr^{-1}$)					CH_3I ($Ggyr^{-1}$)			DMS ($Tgyr^{-1}$)	
	This Study (PWC, N00)	Ziska et al. (2013)	Ordonez et al. (2012)	Liang et al. (2010)	Warwick et al. (2006)	This Study (PWC, N00)	Ziska et al. (2013)	Ordonez et al. (2012)	Liang et al. (2010)	Warwick et al. (2006)	This Study (PWC, N00)	Ziska et al. (2013)	Bell et al. (2002)	This study (PWC, N00)	Lana et al. (2011)
90° –50° N	**1.3**	–4.0	1.6	1.3	0.3	**26.7**	44.8	13.3	9.4	0.9	**13.4**	20.3	14.0	**2.1**	2.3
50° –20° N	**12.5**	16.5	15.3	14.9	10.5	**49.0**	33.9	123.2	108.1	27.9	**36.8**	40.5	89.9	**7.2**	8.5
20° N-20° S	**32.2**	38.4	41.1	34.3	84.5	**108.5**	94.1	286.9	249.0	517.4	**63.3**	59.3	91.2	**18.0**	21.1
20° –50° S	**7.8**	19.3	7.7	9.7	16.5	**41.4**	42.0	98.0	70.5	43.8	**80.7**	67.7	82.4	**13.9**	16.5
50° –90° S	**9.1**	17.2	0.9	1.6	0.9	**12.8**	0.1	7.0	11.6	2.4	**15.5**	17.0	14.9	**4.2**	6.0
Total	**63.0**	87.4	66.6	61.8	112.7	**238.4**	214.9	528.4	448.6	592.4	**209.7**	204.8	291.7	**45.5**	54.4

ACPD
15, 17553–17598, 2015

Table 4. Integrated global emissions during 2010–2011 for sensitivity tests using different parameterizations for the transfer velocity k_w (simulations 3–6, same as in Table 1) and the effects of rain (simulation 7), bubble mediated transfer parametrized using white cap coverage (simulation 8) and parameterizations recently suggested for DMS (simulation 9 and 10). Equations for the parameterizations using wind speed u are given for the Schmidt number (subscript after k) as in the original publications listed. u = wind speed in 10 m a.s.l. in m s^{-1}. If not stated otherwise (i.e. simulation 10), k is given in cm h^{-1}.

No.	Parameterization		CH_2Br_2	$CHBr_3$	CH_3I	DMS
			Gg yr^{-1}	Gg yr^{-1}	Gg yr^{-1}	Tg yr^{-1}
3	Liss and Merlivat (1986)	for $u \leq 3.6$, $k_{660} = 0.17u$ for $3.6 < u < 13$, $k_{660} = 2.85u - 9.65$ for $u \geq 13$, $k_{660} = 5.9u$	53.74	189.10	151.88	33.38
4	Wanninkhof et al. (1999)	$k_{660} = 0.0283u^3$	58.38	211.17	223.52	45.22
5	Nightingale (2000)	$k_{600} = 0.22u^2 + 0.333u$	63.04	238.46	209.73	45.49
6	Ho et al. (2006)	$k_{660} = 0.266u^2$	62.71	236.10	213.47	45.91
7	Ho et al. (2006) + rain	–	65.08	249.66	225.67	48.70
8	White cap coverage	–	62.76	238.51	197.44	42.53
9	Bell et al. (2013), modified	for $u \leq 11$, $k_{600} = 0.22u^2 + 0.333u$ for $u > 11$, $k_{600} = 30.283$	–	–	–	40.63
10	Marandino et al. (2009)	$k_{720} = 0.46u - 0.24$ [m day^{-1}]	–	–	–	42.45
	Mean (simulations 3–6)		59.47	218.71	199.65	42.5

ACPD
15, 17553–17598, 2015

Table 5. Differences in atmospheric concentration for DMS in model runs based on prescribed emissions (PE, simulation set-up 3 in Table 4) and prescribed water concentrations (PWC (N00), simulation 3 and PWC (B13m), simulation 9 in Table 1 and 4). The model output was subsampled at locations and times when measurements were available, and measurements were subtracted from model output to obtain Δ. Total percentages refer to a mean mixing ratio of 180.4 ppt of samples from all listed campaigns (total Δ divided by 180.4). Locations of the ship tracks and the aircraft campaigns (HIPPO 1–5) can be found in Fig. 3. Data referring to the total set of observations are given in bold letters.

	ΔPE [ppt]	ΔPWC (N00) [ppt]	ΔPWC (B13m) [ppt]	ΔPWC (M09) [ppt]
PHASE-I	74.9	69.8	60.3	61.6
Knorr06	−46.7	−112.4	−114.5	−104.30
Knorr07	278.0	146.4	80.7	100.2
M98	440.8	153.0	141.9	172.4
Total ship	**241.6**	**100.8**	**72.0**	**89.3**
HIPPO 1–5	29.0	20.5	13.4	16.3
Total	**86.2**	**42.1**	**29.2**	**35.9**
Total overestimation %	**47.8**	**23.4**	**16.2**	**19.9**

ACPD
15, 17553–17598, 2015

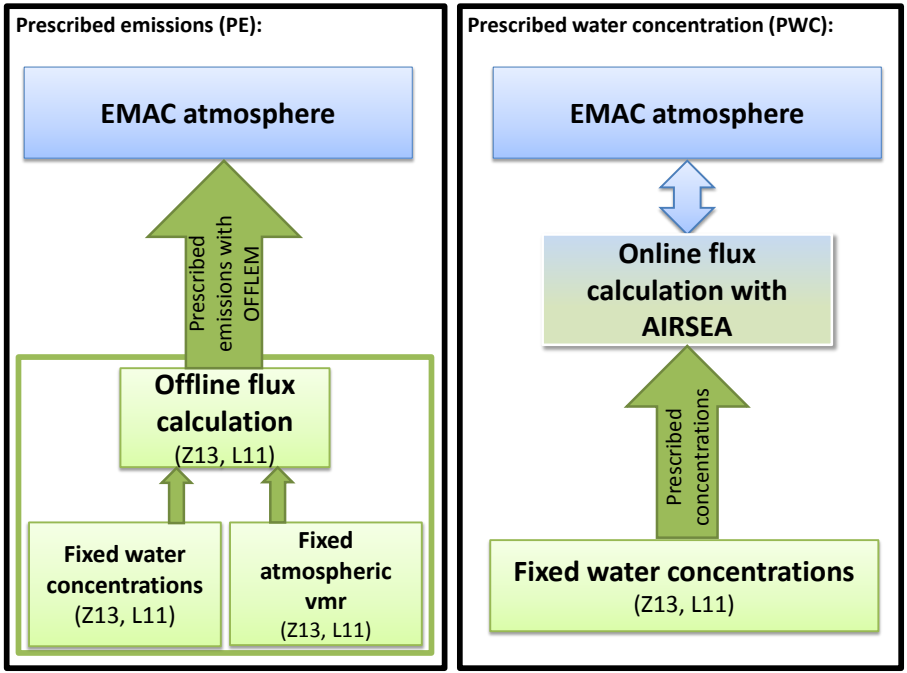

Figure 1. Schematic overview of the set-up of prescribed emissions (PE, left panel) and online calculated fluxes based on prescribed water concentrations (PWC, right panel) implemented in EMAC. Climatologies of fixed water and atmospheric concentrations in Ziska et al. (2013; Z13) and Lana et al. (2011; L11) were used to compute a global emission estimate, and the resulting interannual mean emission climatology is prescribed in EMAC using the submodule OFFLEM (PE, left panel). Calculating emissions online based on prescribed concentration (Z13, L11) considers the current state of the atmosphere during the calculation of emissions in the submodule AIRSEA (PWC, right panel).

ACPD
15, 17553–17598, 2015

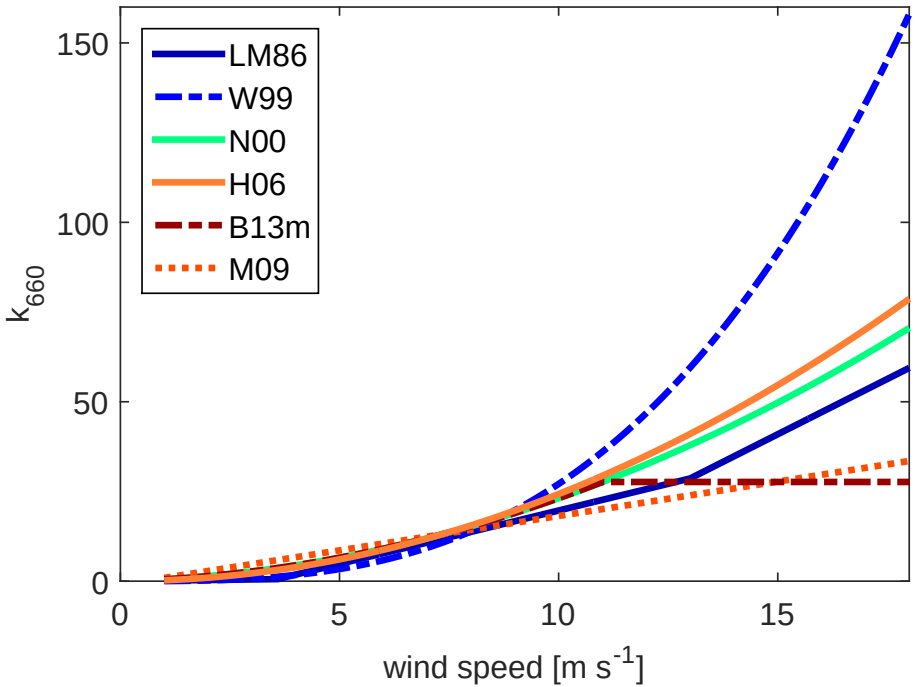

Figure 2. Parameterizations for water-side transfer velocity of air–sea gas exchange k_w for a Schmidt number of 660 that are tested in this study: the linear parameterization LM96 (Liss and Merlivat, 1986), the cubic parameterization W99 (Wanninkhof and McGillis, 1999), the quadratic parameterization N00 (Nightingale et al., 2000) and H06 (Ho et al., 2006), the parameterization modified according to Bell et al. (2013, B13m) with a levelling off at wind speeds higher than 11 m s^{-1}, and the linear parameterization by Marandino et al. (2009, M09).

ACPD
15, 17553–17598, 2015

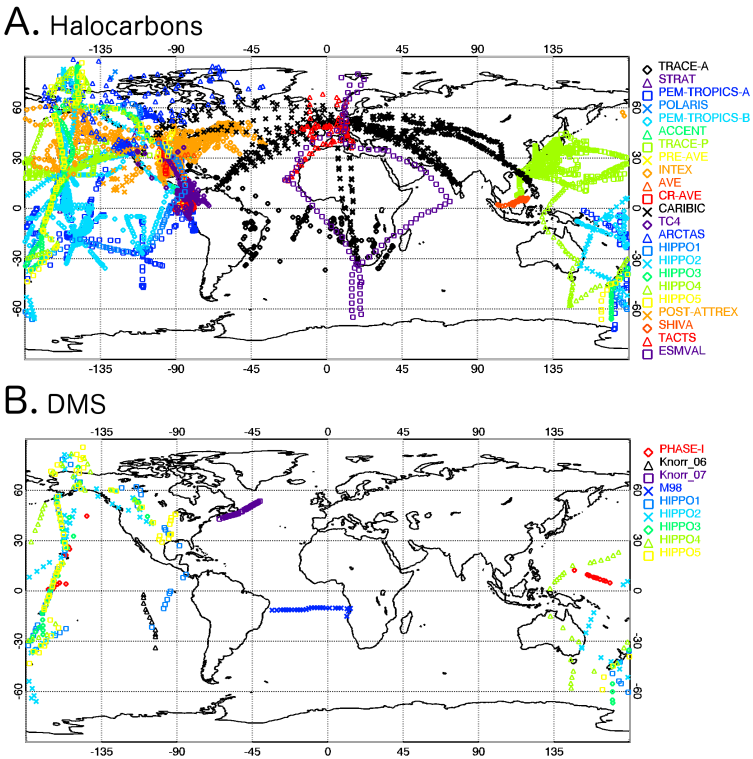

Figure 3. Locations of atmospheric data for comparison with model output used in this study. **(a)** shows locations of atmospheric measurements from 23 aircraft campaigns considered for comparison with halocarbon simulations. **(b)** shows location of measurements in the atmospheric boundary layer from ships (PHASE-1, Knorr-06, Knorr-07, M98) and from aircraft campaigns (HIPPO 1–5) measurements, considered for comparison with DMS simulations.

ACPD
15, 17553–17598, 2015

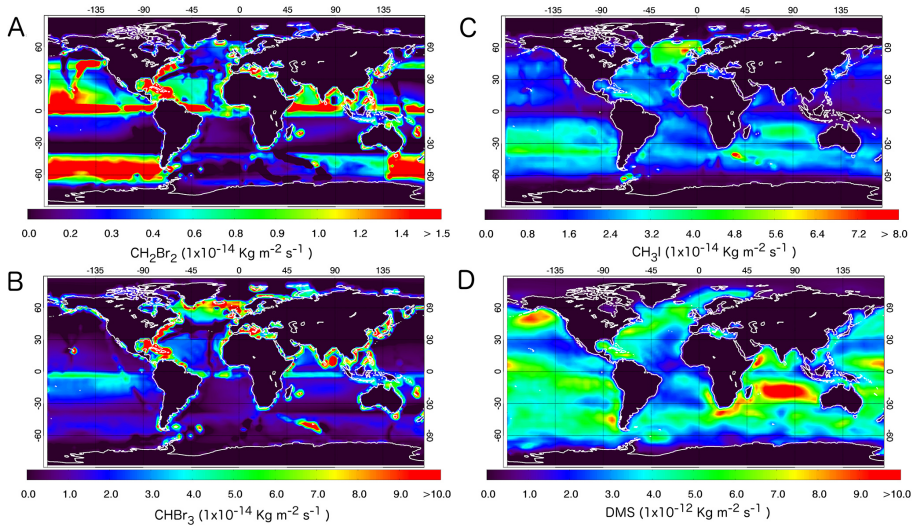

Figure 4. Emissions from prescribed water concentrations (PWC; N00 parameterization for k_w) for the trace gases dibromomethane (CH_2Br_2, **a**), bromoform ($CHBr_3$, **b**), methyliodide (CH_3I, **c**) and dimethylsulphide (DMS, **d**), annual mean of the period 1990–2013 (simulation 1, Table 1).

ACPD
15, 17553–17598, 2015

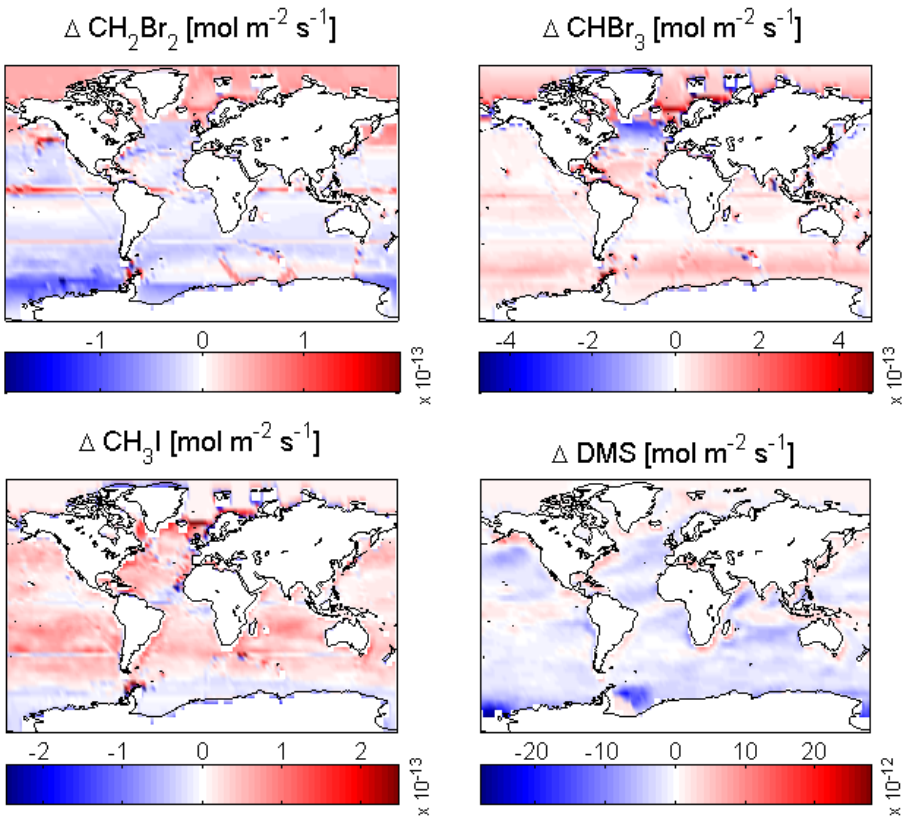

Figure 5. Differences (PWC-PE) in emissions between PWC (simulation 1, Table 1, 2010–2011) and PE (simulation 2, Table 1, 2010–2011). Red indicates a larger flux in the PWC set-up, blue a larger one in the PE set-up.

ACPD
15, 17553–17598, 2015

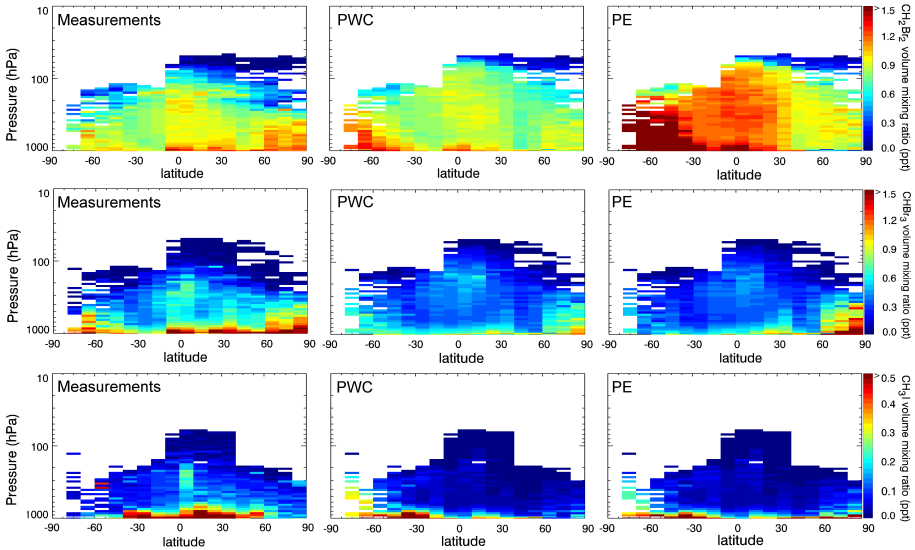

Figure 6. Atmospheric mixing ratios (in ppt) of the trace gases dibromomethane (CH_2Br_2, upper row), bromoform ($CHBr_3$, middle row), and methyliodide (CH_3I, lower row) derived from measurements (see Fig. 3 for locations of aircraft campaigns) and EMAC-runs with prescribed water concentrations and prescibed emissions.

ACPD
15, 17553–17598, 2015

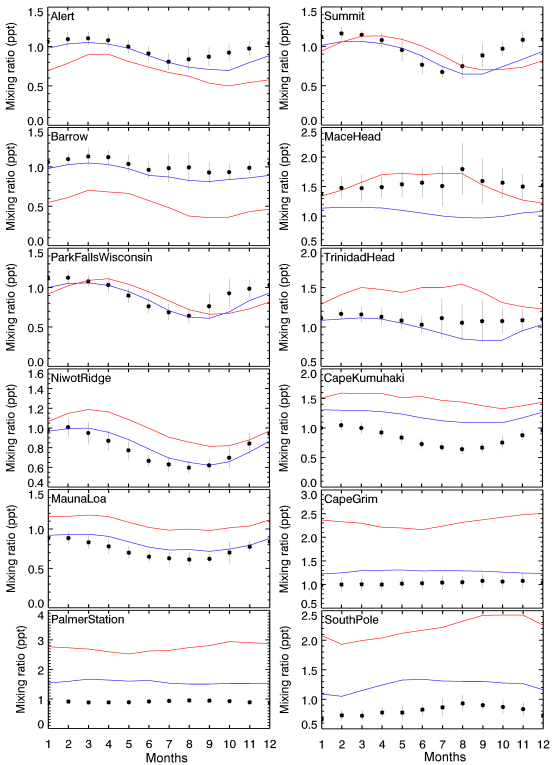

Figure 7. Mean seasonal variation of CH_2Br_2 mixing ratios (in ppt) using model output based on prescribed emissions (PE in red) and prescribed water concentration (PWC in blue), subsampled at the location of the NOAA ground based time series stations. Black dots indicate the long term monthly means of the time series at the specific locations (± standard deviation), vertical lines indicate the corresponding standard deviations.

ACPD
15, 17553–17598, 2015

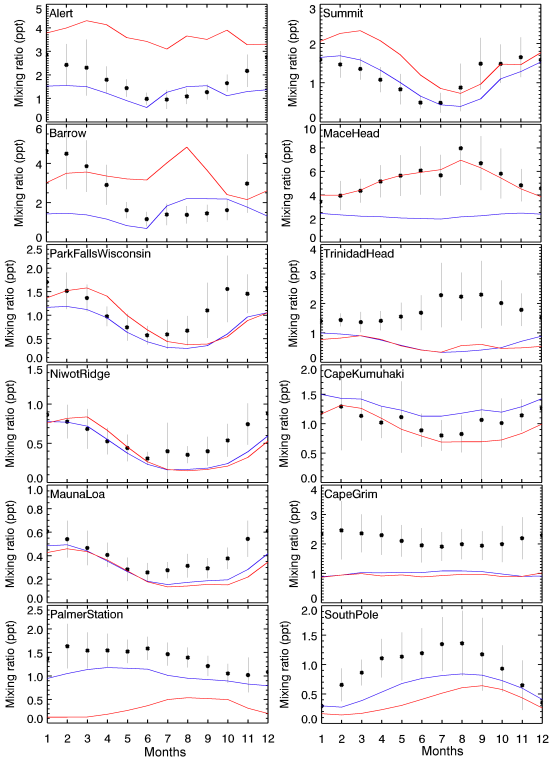

Figure 8. Same as Fig. 7 for $CHBr_3$.

ACPD
15, 17553–17598, 2015

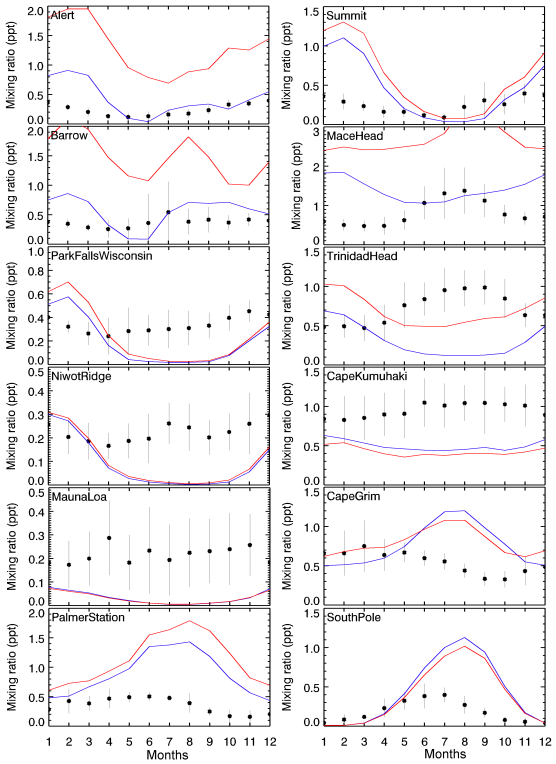

Figure 9. Same as Fig. 7 for CH_3I.

ACPD
15, 17553–17598, 2015

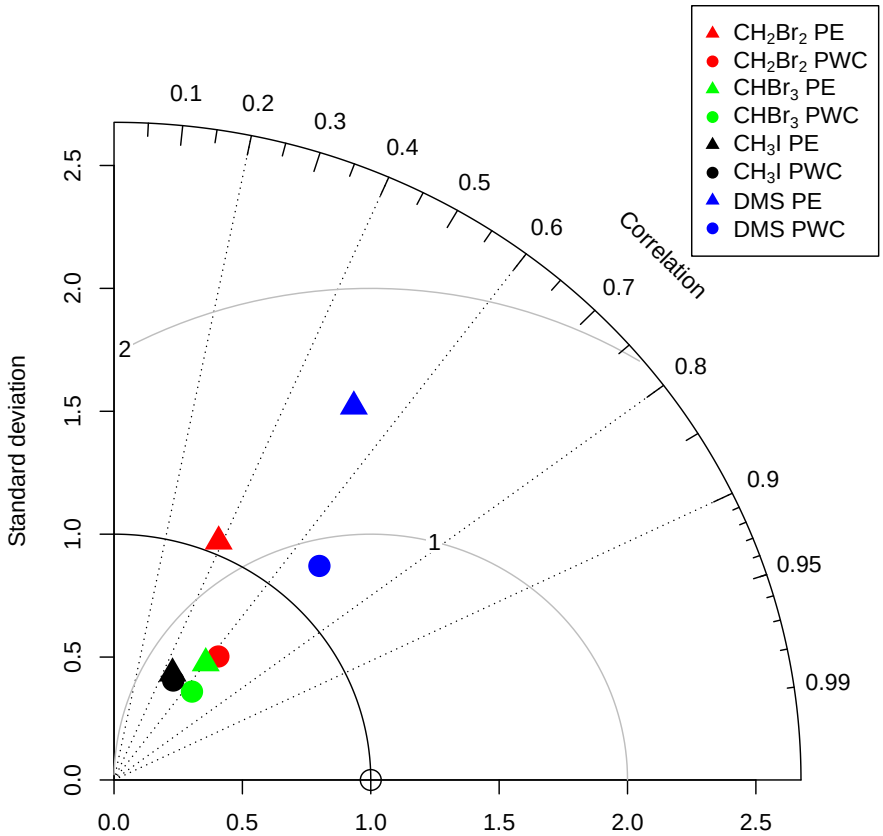

Figure 10. Taylor-Diagram of PE (prescribed emissions, triangles) compared to PWC (prescribed water concentrations, circles) runs using the same parameterization for k_w (N00) for comparison. The Taylor diagram relates model simulations to observations according to their root-mean square error (given as the distance to the reference point, x axis 1.0), correlation and standard deviation. Simulations located closest to the reference point agree best with observations.

ACPD
15, 17553–17598, 2015